From urea to melamine cyanurate: Study of a class of thermal condensation routes for the preparation of graphitic carbon nitride

Pedro Chamorro-Posada [a,*], Roberto C. Dante [b], José Vázquez-Cabo [c], Denisse G. Dante [b], Pablo Martín-Ramos [d], Óscar Rubiños-López [c], Francisco M. Sánchez-Arévalo [e]

[a] *Dpto. de Teoría de la Señal y Comunicaciones e IT, Universidad de Valladolid, ETSI Telecomunicación, Paseo Belén 15, 47011, Valladolid, Spain*
[b] *R&D Department, 2Dto3D S.r.l.s. Via G. Quarello 15/A, 10135 Torino, Italy*
[c] *Dpto. de Teoría de la Señal y Comunicaciones, Universidad de Vigo, ETSE Telecomunicación, Lagoas Marcosende, 36310, Vigo, Spain*
[d] *EPS, Instituto Universitario de Investigación en Ciencias Ambientales de Aragon (IUCA), Universidad de Zaragoza, Carretera de Cuarte s/n, 22071, Huesca, Spain*
[e] *Departamento de reología y mecanica de materiales, Instituto de Investigaciones en Materiales (IIM), Universidad Nacional Autónoma de México (UNAM), Apdo. Postal 70–360, Cd. Universitaria, Mexico City, Mexico*

ARTICLE INFO

ABSTRACT

This work presents a survey of the intermediates in the well-known thermal synthesis of graphitic carbon nitride from urea. The analysis of the crystalline phases depicts a successive transformation of the precursor into different substances previously used as starting reactants, whereby melamine cyanurate arises as the ultimate precursor of a class of thermal condensation routes to obtain graphitic carbon nitride. The study of the optical properties of the synthesized materials evidences the simultaneous production of an amorphous phase with a significant presence of melon oligomers. These results are also supported by the further characterization of the materials performed using THz-TDS, FTIR, HRTEM, and XPS techniques, and by theoretical studies conducted using semi-empirical quantum chemistry methods.

1. Introduction

Graphitic carbon nitride (g-C_3N_4), the result of the 3D structuring of melon polymer layers [1–6], is a highly versatile material with a broad range of applications [7–13]. Melon was first synthesized by Berzelius and Liebig in 1834 [14]. Later, Pauling and Sturdivant elucidated the existence of a C_6N_7 cyameluric nucleus, currently referred to as heptazine or tri-*s*-triazine nucleus [15]. g-C_3N_4 can be obtained by the thermal condensation of a wide variety of nitrogen-rich precursors such as urea [16], thiourea [17], melamine [18], or cyanamide [19]. Li et al. reported the synthesis of carbon nitride by the polycondensation reaction between melamine and cyanuric chloride in presence of nickel powder [20], while Dante et al. based the synthesis on melamine and uric acid [21] and melamine cyanurate [22].

Among the many applications of graphitic carbon nitride, those based on its excellent luminescent properties [23] stand out due to the unique combination of cheap production methods and environmental friendliness. As regards its quantum yield, g-C_3N_4 is outperformed by melem, the melon monomer, with an efficiency one order of magnitude higher [24, 25].

In this work, we revisit the thermal synthesis from urea, one of the simplest precursors in terms of molecular complexity. As opposed to previous works based on different reagents [21,22,26], where the treatment time was kept constant while the products obtained at different temperatures were studied, we now use a fixed temperature and analyze the intermediate products at different reaction times. The analysis of the crystalline phases in the intermediate products unveils a route that is common to a whole class of thermal condensation syntheses, and where melamine cyanurate arises as the ultimate precursor. Whereas this is an important result that brings in some order to a deeply complex matter, the open question of the existence of highly related, yet distinct, synthesis paths becomes even more intriguing.

The global picture, however, is far more complex. The analysis of the UV–Vis absorption, infrared, emission, and terahertz properties of the intermediates indicates the progressive formation of melon oligomers, as an amorphous phase of the material, which occurs in parallel to the transformation of the crystalline phase, and before the eventual condensation of turbostratic graphitic carbon nitride. The interlayer binding of the final 3D-organized graphitic carbon nitride product produces a relevant alteration in the optical absorption properties, much stronger than the milder

---

changes associated with the condensation of 1D and 2D oligomers. The quantum yield of these intermediate oligomers is found to be at an intermediate level between those of pure melem and 3D graphitic carbon nitride. Our survey also highlights the potential of terahertz spectroscopy, an emerging characterization tool, in materials science.

The reaction path in the thermal condensation of g-C$_3$N$_4$ is described in Fig. 1. The analysis of the crystalline phase evidences the transformation from urea to cyanuric acid and melamine cyanurate, the adduct of melamine and cyanuric acid, and, finally, to g-C$_3$N$_4$. At the same time, there is parallel production of amorphous melon oligomers of increasing order.

The analysis presented is twofold, and the experimental results are complemented with a theoretical survey performed using semi-empirical quantum chemistry neglect of diatomic differential overlap (NDDO) methods. The approximations made in these methods are positioned at a degree somewhere in between force-field and ab-initio computations. PM6 and PM7 Hamiltonians are at a performance level commensurate

with density functional theory (DFT) and ab-initio methods when guessing ground state geometries. This accuracy level is obtained at a much smaller computational cost, which allows addressing very large molecular geometries and solid-state systems [27,28]. Semi-empirical computations have proven to be extremely valuable in the theoretical study of the terahertz spectra of materials [3,27,29]. For the theoretical analysis of the optical properties of the materials, we have also used the intermediate neglect of the differential overlap spectroscopic (INDO/S) [30] method with the configuration interaction of singles (CIS) scheme [31,32].

2. Materials and methods

2.1. Materials and synthesis procedure

The precursor material in the synthesis, urea, was supplied by Alfa Aesar. The urea was placed in a crucible and treated in a muffle furnace at
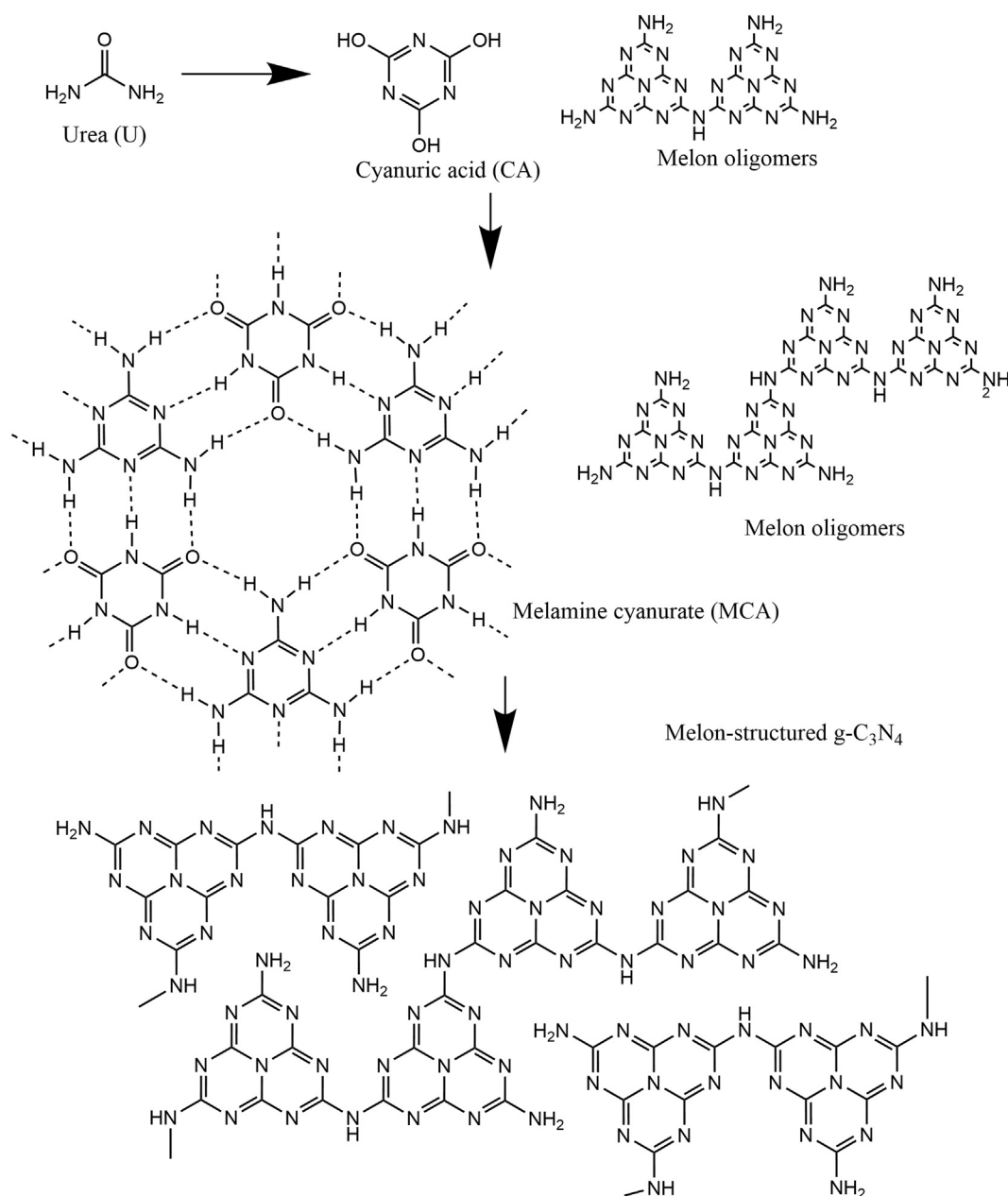

Fig. 1. Reaction path in the thermal condensation route of g-C$_3$N$_4$ addressed in this work, and molecular structure of the materials identified in the reaction process.

450 °C. Four samples were prepared with 15, 30, 45, and 75 min of treatment, respectively. To complete the study, the results of the characterization were compared with relevant additional reference materials: cyanuric acid and melamine were both supplied by Alfa Aesar and melamine cyanurate was supplied by Nachmann S.r.l. The syntheses were carried out under controlled conditions and produced repeatable results.

2.2. Characterization

The powder X-ray diffractograms were measured using a Bruker (Billerica, MA, USA) D8 Discover diffractometer (CuKα = 1.5418 Å).

A Cary 630 spectrophotometer and a UV–Vis Cary 100, in reflection mode, both from Agilent, were used, for the IR spectra (ATR-FTIR) and UV–Vis characterization, respectively.

Scanning electron microscopy (SEM) and transmission electron microscopy (TEM) images were taken using, respectively, an FEI HELIOS NANOLAB 600 at 3, 15 or 20 kV and a JEOL JEM2010F at 200 kV. An Oxford Inca Energy TEM detector was used for the EDS analysis.

The luminescence spectra were measured with an Oxford Instruments FLS980 fluorescence spectrometer. Both emission and excitation measurements were made at 25 °C. Steady-state fluorescence measurements were carried out with a 450 W Xe lamp as a light source and double excitation and emission monochromators. A monochromator at 400 nm was used at the excitation and emission arms. A photomultiplier tube detector cooled by a Peltier system was used for detection. For excitation and emission measurements, the apparatus parameters were: slits widths $\Delta\lambda_{exc} = 0.4$ nm, $\Delta\lambda_{em} = 0.3$ nm, step = 1 nm, dwell = 0.5 s. To measure the photoluminescence quantum yield (QY) the FLS980 fluorescence spectrometer is equipped with an integrating sphere. The measurement conditions of the QY for all samples were: slits widths $\Delta\lambda_{exc} = 2$ nm, $\Delta\lambda_{em} = 0.1$ nm, step = 0.2 nm, dwell = 0.3 s, and 5 repeats.

A Menlo Tera K15 spectrometer was used for the terahertz time-domain spectrometry (THz-TDS) characterization. To prepare the samples, the materials were mixed with polyethylene powder with a concentration of 33 wt% and pressed to form 13 mm diameter pellets with thicknesses ranging between 600 and 900 μm. The spectrometer chamber was purged with nitrogen to avoid the imprint of water in the measurements.

Chemical composition was analyzed through XPS measurements using a Thermo Scientific K-Alpha apparatus. The C1s, O1s, N1s, and survey spectra were acquired at 10^{-9} mbar.

The measurements performed on reference and synthesized samples are consistently identified throughout this work using the same labels and line colors in all the characterizations, namely, urea (U, black), cyanuric acid (CA, green), melamine (M, blue), melamine cyanurate (MCA, red), 15-min treatment sample (15 min, magenta), 30-min treatment sample (30 min, cyan), 45-min treatment sample (45 min, orange), and 75-min treatment sample (75 min, brown).

2.3. Computations

The PM6 [28,33] Hamiltonian in the MOPAC2016 software package was used for the quantum chemistry computations in an Intel Xeon E5-1650v2 6-core (12 threads) 3.5 GHz server running a Linux operating system. The PM6 optimized geometries were used for the calculation of the electronic spectrum using the intermediate neglect of differential overlap/spectroscopic (INDO/S), configuration interaction with singles (CIS) method [34,35], as implemented in the ORCA package, version 2.9.1 [36].

3. Results and discussion

The largely studied [16] synthesis of carbon nitride from urea has some sort of fundamental character due to the simplicity of the precursor. In this work, we address the chain of intermediates observed in this synthesis route. For this purpose, the initial reagent was placed in a crucible and heated at 450 °C for different time durations. Fig. 2 displays
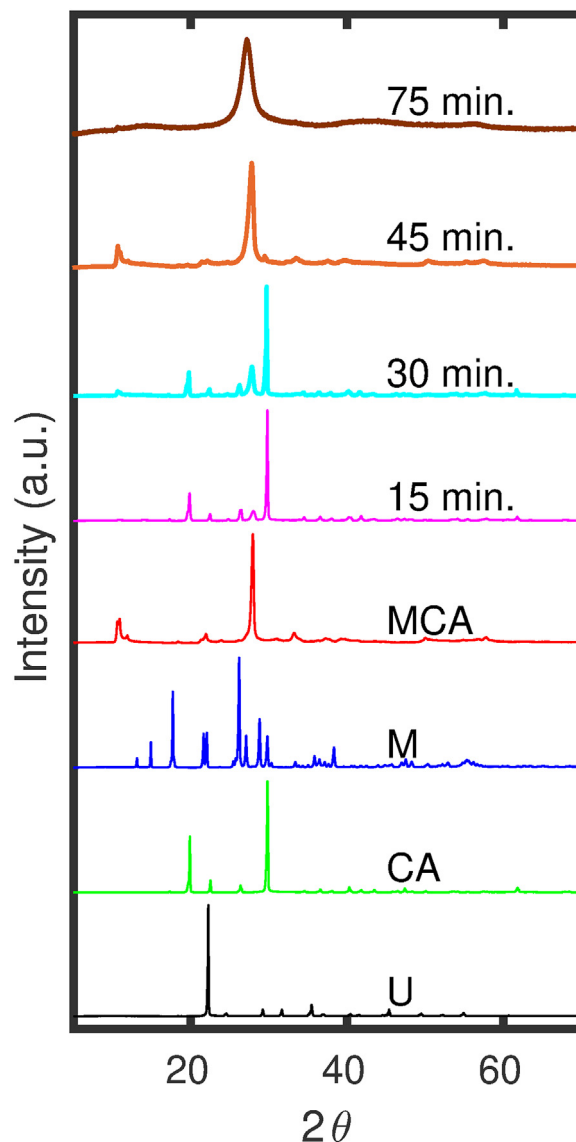

Fig. 2. Diffractograms of the samples obtained by heating urea at 450 °C during 75, 45, 30, and 15 min, and those of the reference high purity samples of urea (U), cyanuric acid (CA), melamine (M), and melamine cyanurate (MCA).

the powder diffractograms of the samples obtained, together with those of several reference materials: the precursor, urea; cyanuric acid; melamine cyanurate; and the second component of the MCA complex, melamine. We note that all these materials have been employed as precursors in various thermal condensation synthesis procedures of graphitic carbon nitride.

The observation of the results presented in Fig. 2 determines the complete formation of graphitic carbon nitride, g-C_3N_4, after 75 min treatment, as heralded by the peak at $2\theta = 27.2°$ corresponding to stacking of layers with a separation of 3.37 Å. The comparison of the diffractograms of the intermediate samples obtained after 15, 30, and 45 min of treatment with those of the reference materials reveals that the crystalline phase in the samples obtained at 15 and 30 min corresponds to CA, whereas the XRD pattern of the last intermediate, at 45 min, gives an excellent match of the crystalline phase to the XRD signature of MCA. It is also noteworthy the proximity of the main peak in the MCA diffractogram ($2\theta = 27.94°$, $d = 3.29$ Å) to that of the completely structured g-C_3N_4 at the 75-min sample.

There is a wide variety of nitrogen-rich substances that lead to the eventual formation of graphitic carbon nitride via thermal condensation.
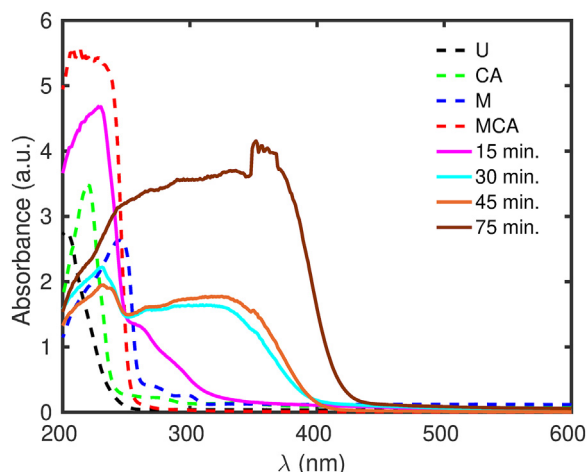
Fig. 3. UV–Vis absorbance (in terms of the K-M absorbance units) of the samples synthesized by thermal condensation of urea at 450 °C during 15, 30, 45, and 75 min (with solid lines) and those of the reference pure samples (with dashed lines) of urea (U), cyanuric acid (CA), melamine (M) and melamine cyanurate (MCA).
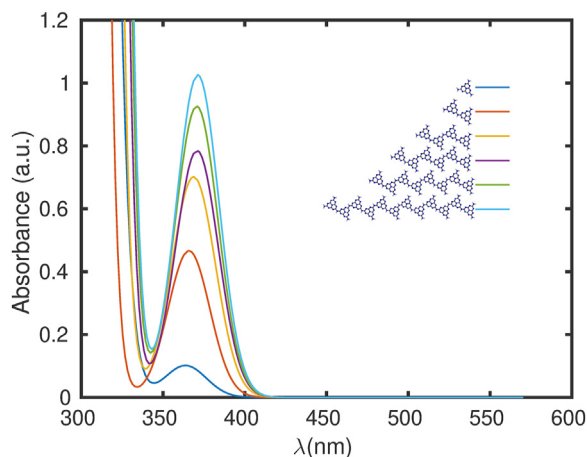

Fig. 4. Calculated UV–Vis spectra of the melon oligomers using the INDO/S method and ground states geometries optimized with the PM6 Hamiltonian. Absorption intensities have been normalized to the number of heptazine units in the oligomer.

These include, besides our precursor, U, the intermediates sequenced in the crystalline phase: CA and MCA. Our observation of the crystalline phases in the synthesis from urea, summarized in Fig. 2, permits us to trace a series of synthesis routes belonging to the same class, where the
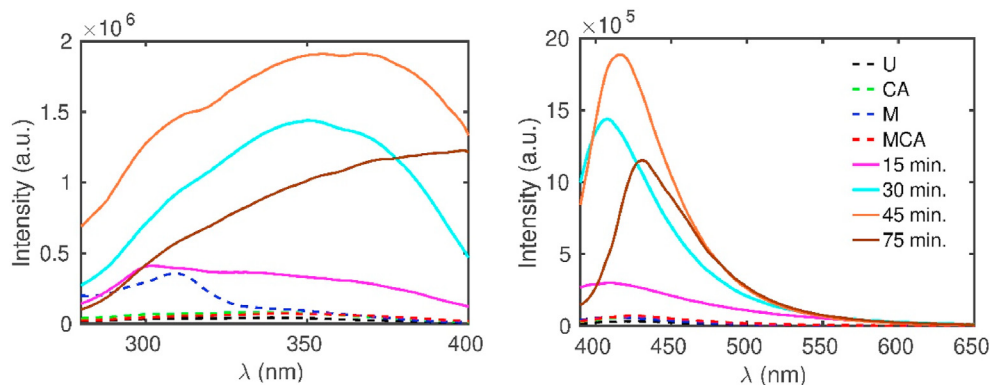
last step, MCA, plays the role of ultimate precursor. Nonetheless, further analyses of the synthesized materials and the corresponding pristine reference substances reveal very interesting properties of the intermediates aside from those of the crystalline phases.

Fig. 3 displays the UV–Vis absorption spectra of the synthesized and reference powder samples. The absorbance has been obtained from the diffuse reflectance of the sample R using the Kubelka-Munk function $F(R) = (1 - R)^2/(2R)$. After 75 min of treatment, the absorption spectrum is consistent with that of properly conformed graphitic carbon nitride, with a band-gap close to 3 eV [3,5]. Hence, there is a very good correspondence between the XRD and optical absorption data as regards the final synthesized product. The conclusion is drastically different when the results of the intermediate products are analyzed. The X-ray diffraction patterns indicate the presence of CA in the 15- and 30-min samples, and MCA in the 45-min sample. Nevertheless, the absorption spectra displayed in Fig. 3 show remarkable differences between the synthesized materials and the corresponding pure substances, with notably red-shifted band-gaps in the synthesized materials when compared to those of the pristine reference materials.

An explanation for this apparent discrepancy is provided by theoretical analyses employing semi-empirical quantum chemistry methods. The progressive shift of the absorption band-gap of melon oligomers was previously addressed in [3] as part of the process in a conventional extrapolation method for the estimation of polymer band-gaps [37,38]. These analyses show a very mild variation of the edge of the excitation spectra as the melon oligomer order grows. On the other hand, the formation of 2D polymer sheets by the hydrogen bond linkage of 1D melon chains by hydrogen bonds does not produce relevant shifts of the optical band-gap [3]. These results can be interpreted [3,39] as the result of the effective electronic isolation of the heptazine units in 1D and 2D melon arrangements. Fig. 4 displays the reconstructed absorption spectra resulting from the INDO/S calculations for different oligomer orders normalized to the number of heptazine units in the molecular arrangements. The results for the fundamental melem unit are also shown. Besides the progressive shift of the optical band-gap, we observe an increase of the expected absorbance with the oligomer order.

The calculated results account for the aforementioned illusive divergence in the XRD and UV–Vis measurements displayed, respectively, in Figs. 2 and 3. Aside from the transformation of the initial reagent following the U→CA→MCA chain that eventually leads to the complete production of graphitic carbon nitride, there exists an accompanying early formation of 0D melem, and 1D and 2D melon units. In this scenario, the absorption spectrum of the 15-min sample in Fig. 3 corresponds mainly to the nascent production of melem and very low order melon oligomers, whereas the 30- and 45-min products indicate that the transformation of the initial reagents towards the MCA is accompanied by the production of increasing size well conformed 2D polymer sheets. The theoretical analyses predict small variations of the optical spectra as the condensation of the 2D phase progresses, consistent with the measurements performed on the 30- and 45-min samples. There is also a very

Fig. 5. (*Left*) Excitation and (*right*) emission spectra. The emission spectra have been characterized upon excitation at 365 nm, and the excitation spectra at the maximum emission wavelength of each sample. Results are presented for the samples synthesized by thermal condensation of urea at 450 °C during 15, 30, 45, and 75 min (with solid lines) and those of the reference pure samples (with dashed lines) of urea (U), cyanuric acid (CA), melamine (M), and melamine cyanurate (MCA). Legend has only been included in the plot on the right, but the curve labels are the same for both graphs.

good agreement between the spectral position of the predicted lowest energy absorption band in Fig. 4 and the measurements of these 1D and 2D phases shown in Fig. 3. On the other hand, the strong inter-layer electron interactions in the final graphitic carbon nitride product (75-min sample) with a full 3D formation (as observed from the XRD measurements) have a notable impact on the optical absorption spectrum depicted in Fig. 4. Therefore, the analysis of the intermediates produced in the synthesis of g-C_3N_4 permits the full reconciliation of the theoretical predictions of the absorption spectra of these substances with the measured data. In previous works [3,39], the apparent discrepancy was misinterpreted as the result of a small inaccuracy of the theoretical predictions.

The analysis of the absorption properties displayed in Figs. 3 and 4 shows, in good agreement with the theoretical predictions, that once a certain degree of condensation of the 2D phase has been achieved, further consolidation of the sheets has little effect on the absorption properties of the material, as indicated by the curves corresponding to 30- and 45-min samples. The situation is different as regards the luminescence properties. It is important to highlight that the band-gaps of the pure samples of U, CA, and MCA are far from the excitation wavelength employed (365 nm), as shown in the absorption spectra of Fig. 3, which guarantees a negligible impact from the crystalline phases on the luminescence properties of the samples and effectively isolates the study on the amorphous phases based on the luminescence properties. Fig. 5 displays the emission and excitation spectra of the synthesized and reference samples. A wide variation in the luminescence response can be observed in the synthesized samples, with the strongest response, at the chosen excitation wavelength, from the 45-min sample. Also, in good accordance with the measurements previously performed on the absorption spectra that show that the bandgaps of all the pristine reference materials are largely shifted to the ultraviolet end of the spectrum, an extremely weak luminescence under the excitation wavelength is observed in all the reference samples. The measurement of the luminescence quantum yield (QY) of the four synthesized samples gives 21.29%, 8.55%, 12.08%, and 5.47% for the samples after treatment for 15, 30, 45, and 75 min. The QY of the 75-min sample is very similar to previously reported values for bulk g-C_3N_4 [24], 4.80%, and confirms the full transformation into the final product observed in the XRD measurements. In spite of the observation of a lower luminescence response, the highest QY observed for the 15-min sample is well correlated with the also small absorption at the excitation wavelength. The measured QY is close to the previously reported value for ordinary melem [24], 35.16%, and we can attribute the observed optical response to the nascent production of the melon monomer, in a relatively small concentration, after 15 min of treatment. As regards the samples obtained after longer thermal treatments, we obtain intermediate values between those of pure melem and the final g-C_3N_4, with a larger value of the QY after 45 min of treatment. We connect these results with the progressive generation of 1D and 2D melon oligomers in this temporal range.

THz-TDS is a very useful characterization method, especially well-suited for crystalline materials with long-range vibration modes, which typically produce neat resonance peaks [27]. Nevertheless, this technique has also proven to be extremely convenient in the analysis of layered materials when these types of vibrations are present either in the 3D or the 2D phase [3,29], i.e., with and without strong inter-layer interactions, respectively. For materials with a low degree of crystallinity, the terahertz spectrum typically displays a loosely defined absorption signature that monotonically grows with frequency. Nevertheless, when related materials of this type are analyzed, and there exists a spatially extended vibration mode typical of this spectral region, the careful analysis of these apparently poorly defined absorption features provides very useful information on the degree of organization of the layered structure. This is the case, for instance, in the classification of different types of graphites according to their structural ordering using the terahertz response [29]. In graphite, the existence of a vibration mode characteristic of the 3D arrangement provides an enhancement of the
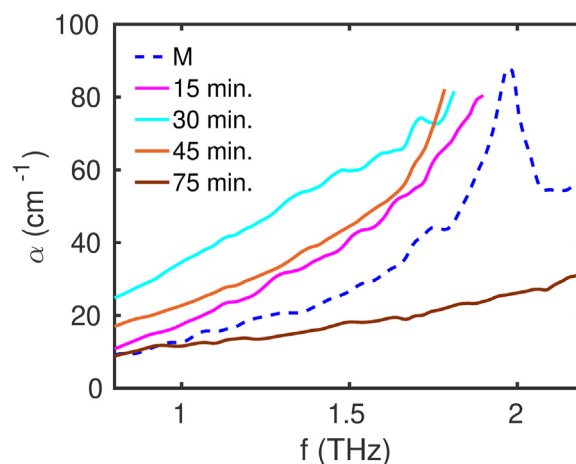

Fig. 6. Terahertz attenuation spectra of the samples prepared with 15, 30, 45, and 75 min of treatment of urea at 450 °C measured using THz-TDS. The measurement of a pristine melamine sample is also included, with a dashed trace, as a reference.

terahertz attenuation correlated with the inter-layer structural organization. In the case of polymeric carbon nitride [3], on the contrary, it is the 2D phase the one that exhibits a series of vibration modes, with a peak response close to 1.8 THz, which are quenched in a full 3D organization. Therefore, the increase of the structural order and the inter-layer interactions is anti-correlated with the terahertz attenuation.

The terahertz spectra of the synthesized samples are shown in Fig. 6. Instead of absorbance units, A, the plots display attenuation coefficient data, α, related to the former as $A = \alpha L$, where L is the sample thickness. This permits a fair comparison of samples with varying signal propagation paths L. These data have been obtained from the time-domain photocurrent traces at the spectrometer's receiving antenna, which are shaped not only by the materials' parameters but also from the etalon effect due to reflections at the sample-air interfaces. The signal processing performed on the photocurrent data to obtain the material parameters is similar to that discussed in [40]. In the analysis of THz-TDS signals from low crystallinity samples, the reduction of the dynamic range at the high-frequency edge of the spectrum can carve the measured broad spectral bands typical of disordered materials, producing an artifact resembling a resonant peak [41]. Therefore, the absorption traces in Fig. 6 have been truncated to avoid this artifact. For reference purposes, the measured spectrum of a pristine melamine sample has also been included. As it is well-known, this substance displays a well-defined peak at 2 THz [42]. The plotted results show a slight frequency down-shift of this resonance due to the dynamic range limitations of the spectrometer.

The analysis of the synthesized samples with different treatment times shows a growth of the attenuation from the 15-min to the 30-min samples. The 45-min sample displays an attenuation smaller than that of the 30-min sample at the lower frequency range, but the slope of the curve increases as the 1.8 THz region is approached, and attenuation eventually takes over that of the 30-min curve. The curve of the 75-min sample, with the full transformation into the final graphitic carbon nitride product, shows a drastically reduced attenuation. Therefore, the THz-TDS data are fully consistent with the interpretation of the non-crystalline phases in the various samples deduced from the optical properties, where the evolution of the crystalline phase is accompanied by partial condensation of 1D and 2D melon intermediates. The measurements at 15- and 30-min indicate the progressive formation of an amorphous phase compatible with the presence of low-order melon oligomers, as evidenced by the luminescence measurements and, possibly, additional −also amorphous− intermediate substances, as indicated by the XPS characterization discussed below. The 45- and 75-min measurements evidence the progressive organization of the material in larger melon sheets and the final production of melon-structured g-
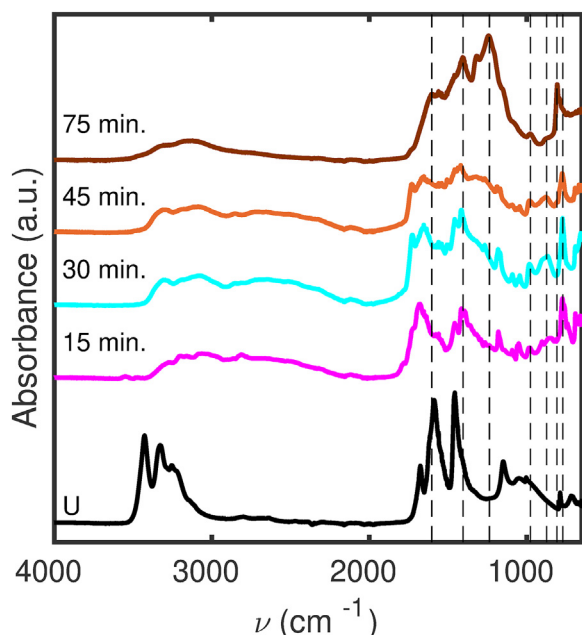
Fig. 7. Infrared spectra of the urea sample 'as-is' (U), and after treatment at 450 °C for different times. Vertical dashed lines mark the resonances at (*from left to right*) 1603, 1404, 1237, 976, 874, 808, and 770 cm^{-1}.

C_3N_4, with strong interlayer interactions that hamper the long-range vibration mode characteristic of 1D and 2D melon arrangements [3].

The infrared spectra of carbon nitride intermediates synthesized with urea are presented in Fig. 7, while the infrared spectrum of carbon nitride itself has been discussed in detail in several previous research reports [3, 22,26]. The spectrum of urea is characterized by the bands of C=O stretching around 1700 cm^{-1}, the N–H bending between 1600 and 1450 cm^{-1}, and the N–H stretching between 3500 and 3100 cm^{-1}. These bands are still present in the intermediates after 15, 30, and 45 min (Fig. 7), while they disappear in the 75-min sample that can be considered a fully-formed g-C_3N_4. On the other hand, the bands relative to g-C_3N_4 are growing, especially the one related to the secondary bridging amine at 1237 cm^{-1}. It is also noteworthy the presence in the 45-min sample of bands corresponding to melamine cyanurate, as shown in
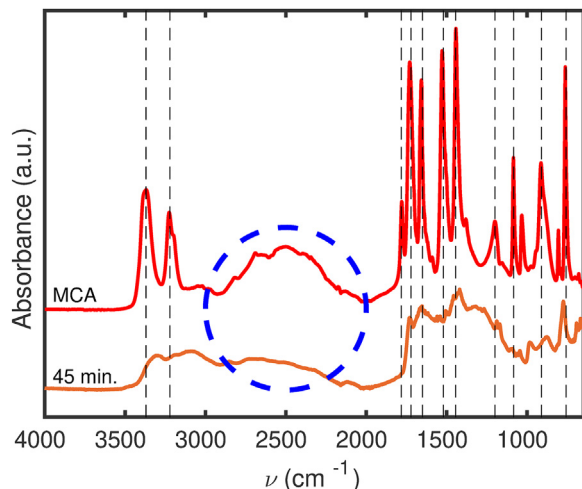

Fig. 8. Comparison of the infrared spectra of the complex of melamine cyanurate (MCA), and the sample of urea treated at 450 °C for 45 min. The dashed lines mark the main bands of melamine cyanurate at (*from left to right*) 3370, 3221, 1782, 1722, 1650, 1521.1199, 1083, 911, and 757 cm^{-1}, while the circle highlights the H-bond region.

Fig. 8. Considering that the secondary bridging amine is not well-developed, it is probable that −apart from melamine cyanurate− melon oligomers prevail, conferring the characteristic luminescence properties.

It should also be pointed out that the peak 808 cm^{-1} in Fig. 7, arising from bending modes of the tri-*s*-triazine units, can be related to long chains, while the band at 874 cm^{-1} should be related to short chains, as discussed in a previous research report [46]. Therefore, the increase in the relative intensity of the peak at 808 cm^{-1} in the 75-min sample may be ascribed to the prevalence of longer chains. The band at 808 cm^{-1} appears markedly in the 75-min sample, while in the samples treated for shorter times the band at 874 cm^{-1} prevails, in agreement with the predominance of oligomers. The broad band centered at 2500 cm^{-1} in the hydrogen bond region was evidenced in both melamine cyanurate and the sample treated for 45-min, which indicates that the complex of melamine cyanurate is an important intermediate in the formation of g-C_3N_4, although it is mixed with all other intermediates. The formation of triazines (cyanuric acid and melamine in the adduct) is highlighted by the presence of the band around 770 cm^{-1}, which is attributable to the triazine bending mode (Figs. 7 and 8). Summing up, all the IR data are compatible with the development of a well-formed carbon nitride through several steps: starting from the formation of the intermediate complex of melamine cyanurate, then passing from short chains to longer chains of melon, to finally yield g-C_3N_4. The determining factors are temperature and time; in fact, at the given temperature of 450 °C, all the stages can be detected in continuous succession.

Electron microscope images from the sample synthesized after 45 min of thermal treatment are shown in Fig. 9. The SEM images in the top row of Fig. 9 display a general view of a flake of the material. The second row shows TEM images of a section of the flake where, as expected, it can be appreciated the presence of both an amorphous phase and granular inclusions that are assigned to MCA crystallites. The detailed reaction path in a specific thermal condensation route of graphitic carbon nitride imprints on the final material its peculiar morphology, which can widely vary among synthesis paths [6]. Even marked differences in the physical and chemical properties depending on the reaction chain can be observed [43]. Although graphitic carbon nitride has not yet been formed in the sample after 45 min of treatment, in the TEM images it can be observed that the morphology of the amorphous phase consists of large layers with wrinkles and pores on the surface, consistent with that reported by [44] for g-C_3N_4 nanosheets synthesized through urea polymerization in Ar atmosphere at the same temperature (given that at higher temperatures cracking and rolling into smaller atrium-like segments occurs). According to [45], who also studied by SEM and HRTEM samples of g-C_3N_4 prepared from different precursors, carbon nitride prepared from urea has a distinctive structure due to gas-release during thermal polymerization, which generates ultrathin 2D sheets (in the heating stage, urea condenses and releases NH_3, H_2O, and CO_2 at the same time, which results in the formation of a thin, porous layered material). The third row in Fig. 9 (left) permits the identification of the layered arrangement in one of these crystalline inclusions. The image on the right displays the results from the selected area electron diffraction (SAED) analysis, showing a diffraction signature corresponding to an interlayer spacing of 3.28 Å, in good agreement with that of MCA obtained from XRD measurements. These crystalline domains are analyzed in more detail in the HRTEM images displayed in the fourth row in Fig. 9, in which the lattice fringes can be clearly seen, confirming the interlayer spacing obtained from SAED data.

The survey spectrum of XPS of the sample treated for 45 min is displayed in Fig. 10, and Table 1 shows the atomic concentration of carbon, nitrogen, and oxygen. The deconvolution of the C1s, N1s and O1s peaks and the attribution to different atomic species are displayed in Fig. 11 and Table 2. The elementary species present in the sample are consistent with the interpretation of the material as a mixture of, at least, MCA crystallites and 1D and 2D melon oligomers. If we attributed the whole oxygen content to the MCA crystalline phase, the result would be a very
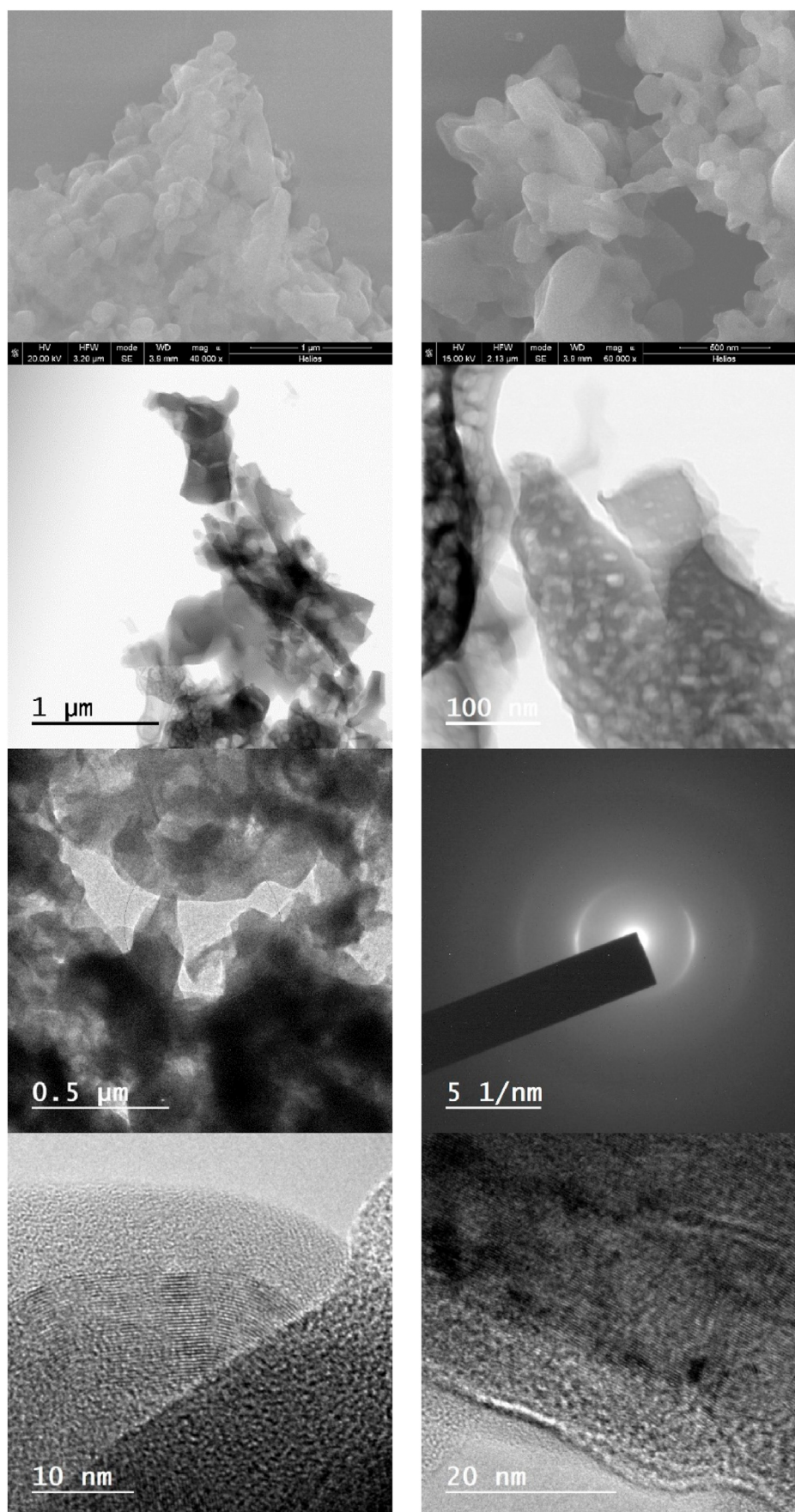
Fig. 9. Electron microscopy results for the sample treated during 45 min at 450 °C: SEM measurements (*top row*), TEM results (*second row*), electron diffraction (*third row*), and HRTEM (*fourth row*).
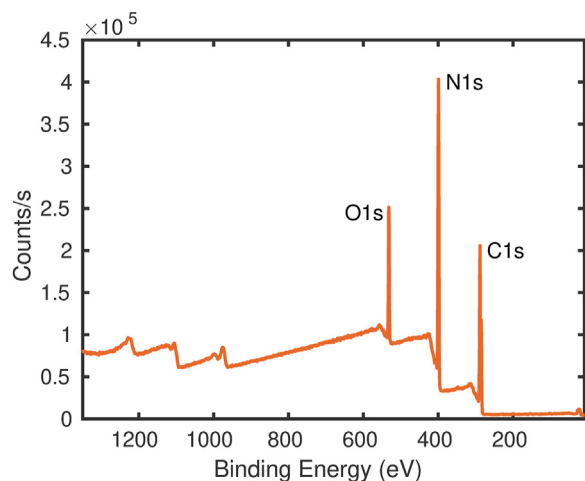
Fig. 10. Survey of the sample treated during 45 min at 450 °C.

Table 1
Data from the survey spectrum with the atomic percentage of detected elements.

Name	Peak BE	FWHM eV	Area (P) CPS.eV	Atomic %
C1s	288,19	2,6	718823,34	47,09
N1s	399,21	3,05	1077181,04	41,56
O1s	531,85	2,63	442895,14	11,35

high contribution of MCA to the total composition of the material. Nevertheless, the remaining carbon and nitrogen would be in a proportion far from the relation close to 1:1.5 expected from long-chain melon oligomers, indicating the existence of additional substances besides MCA and melem oligomers. XPS measurements also show a significant contribution from sp3 nitrogen widely exceeding the yet abundant expected contribution from the amino groups bridging the polymer. If we focus on the C sp2 and N sp2 species, we find a 1.375 nitrogen/carbon ratio, while the expected value for the polymeric carbon nitride is 1.5. If the sample were a perfect mixture of fully synthesized polymer and melamine cyanurate, this data would indicate that melamine cyanurate would account just for 12.5% of the molar content. This indicates that the 45-min sample is a blend of compounds with nitrogen/carbon ratios ranging from the value of 1 of melamine cyanurate and passing, through intermediates with growing values of this ratios, to the well-formed

Table 2
Atomic concentrations of C1s, N1s, and O1s species and the positions of the peaks.

Name	Peak BE	FWHM eV	Area (P) CPS.eV	Atomic %
C1s C–C, C–H	284,80	1,26	24237,71	26,85
C1s C–O–C, C–O–H	285,82	1,53	7070,15	7,84
C1s N-sp3	288,31	1,44	40476,64	44,92
C1s N-sp2	289,33	1,38	18363,98	20,39
Total				100%
N1s N sp3	398,78	1,35	63537,64	47,35
N1s N sp2	399,83	1,23	42538,92	31,72
N1s N-(C═O)	400,81	1,22	28057,16	20,93
Total				100
O1s C–O–C, C–OH	531,93	2,08	55286,51	100

polymer. The C and N sp3 probably belong to compounds that, by decomposition, leave the reaction environment.

There exists a wide variety of nitrogen-rich substances that, under thermal treatment above a certain temperature, lead to the eventual formation of graphitic carbon nitride through different reaction paths. It has been reported [47] the existence of a well-defined class of such synthetic routes that share the production of melem [24] as an intermediate. The course to melem can be direct, using non-metal tricyanomelaminates as initial reagents [48], or through melamine, acting either as the synthesis precursor [18] or as an intermediate. The presence of melamine in the synthesis route defines a subclass of this family including paths where dicyandiamide and its salts act as initial reagents [49]. At the same time, this sub-class of paths includes the possible formation of melam as an intermediate, depending on the synthesis temperature [50].

By analyzing the chain of intermediates in the reaction path of the thermal synthesis of g-C₃N₄ from urea, we have established the probable linkage defining another class of thermal condensation paths that share the presence of melamine cyanurate, either as the precursor or an intermediate in the synthesis. This class, where MCA plays the role of ultimate intermediate, includes various materials that, when used as initial reagents, eventually lead to the formation of graphitic carbon nitride. These include urea [16], the melamine cyanurate adduct [22], and mixtures of cyanuric acid and melamine [51], uric acid and melamine [52] −through the transformation of uric acid to cyanuric acid−, and urea plus cyanuric acid and melamine [53].

4. Conclusion

We have revisited the well-known synthesis of graphitic carbon nitride from urea focusing on the sequence of the intermediates obtained
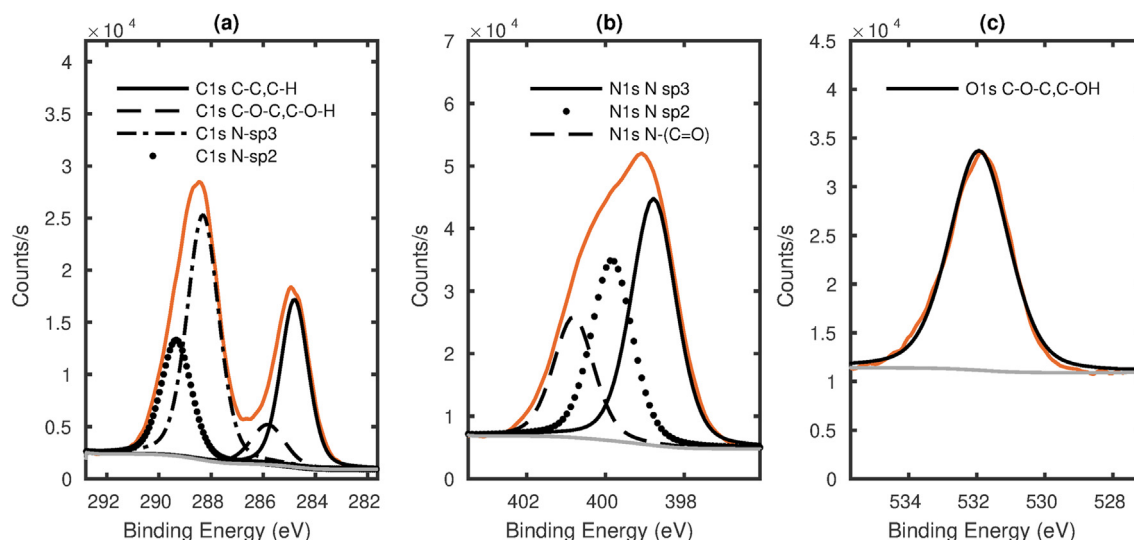

Fig. 11. Deconvolution of the C1s, N1s, and O1s peaks: (a) C1s scan, (b) N1s scan, and (c) O1s scan.

in the process by observing the products obtained at different reaction times. The analysis of the crystalline phases indicates the existence of a well-defined sequence starting with the formation of cyanuric acid, after 15–30 min of treatment, and followed by the transformation into melamine cyanurate (MCA) after 45 min, prior to the generation of the final product at 75 min. These three substances, individually, have been used for the production of g-C_3N_4 via thermal condensation. Therefore, our study unifies the syntheses from these reagents into a single class where MCA is the ultimate precursor. This result brings some order to the thermal generation of g-C_3N_4 from nitrogen-rich materials. Nevertheless, the fact that very closely related substances can be used in this type of synthesis following widely diverging paths is compelling and deserves further scrutiny.

The complexity of this subject is best illustrated by the results of our analyses performed on the non-crystalline phases in the intermediates. In particular, the presence of melon oligomers is witnessed by the optical absorption and emission properties of the synthesized materials. The wide separation of the band-gap of the crystalline substances from the excitation wavelength guarantees a negligible interference from these materials. Both melon and melem are of high interest as metal-free, environmentally-friendly chromophores, suitable for cheap industrial mass-production. We find that the melon oligomers have an intermediate QY between those of melon and melem that grows with the complexity of the compound. The analyses of the optical absorption are in excellent agreement with our theoretical predictions. HRTEM analysis confirms the picture depicted above, and the presence of MCA crystallites before the full production of g-C_3N_4. Measurements of the infrared and far-infrared vibrational spectra provide a full picture of the chain of transformations of the whole material combining crystalline and amorphous phases.

CRediT authorship contribution statement

Pedro Chamorro-Posada: Conceptualization, Investigation, Writing – original draft. **Roberto C. Dante:** Conceptualization, Investigation, Writing – original draft. **José Vázquez-Cabo:** Investigation. **Denisse G. Dante:** Investigation. **Pablo Martín-Ramos:** Investigation, Writing – review & editing. **Óscar Rubiños-López:** Investigation. **Francisco M. Sánchez-Arévalo:** Investigation.

Declaration of competing interest

The authors declare that they have no known competing financial interests or personal relationships that could have appeared to influence the work reported in this paper.

Acknowledgement

References

[1] B.V. Lotsch, M. Döblinger, J. Sehnert, L. Seyfarth, J. Senker, O. Oeckler, W. Schnick, Unmasking melon by a complementary approach employing electron diffraction, solid-state NMR spectroscopy, and theoretical calculations—structural characterization of a carbon nitride polymer, Chem. Eur J. 13 (2007) 4969–4980.

[2] R. Su, Metal-free functionalised carbons in photocatalysis, in: A. Villa, N. Dimitratos (Eds.), Metal-free Functionalized Carbons in Catalysis, The Royal Society of Chemistry, Croydon (UK), 2018, pp. 279–286.

[3] P. Chamorro-Posada, J. Vázquez-Cabo, F.M. Sánchez-Arévalo, P. Martín-Ramos, J. Martín-Gil, L.M. Navas-Gracia, RobertoC. Dante, 2D to 3D transition of polymeric carbon nitride nanosheets, J. Solid State Chem. 219 (2014) 232–241.

[4] P. Chamorro-Posada, P. Martín-Ramos, F.M. Sánchez-Arévalo, R.C. Dante, Molecular dynamics simulations of nanosheets of polymeric carbon nitride and comparison with experimental observations, Fullerenes, Nanotubes, Carbon Nanostruct 26 (2018) 137–144.

[5] P. Chamorro-Posada, R.C. Dante, J. Vázquez-Cabo, D.G. Dante, P. Martín-Ramos, O. Rubiños-López, F.M. Sánchez-Arévalo, Experimental and theoretical investigations on a CVD grown thin film of polymeric carbon nitride and its structure, Diam. Relat. Mater. 111 (2021) 108169.

[6] A. Thomas, A. Fischer, F. Goettmann, M. Antonietti, J.-O. Müller, R. Schlögl, J.M. Carlsson, Graphitic carbon nitride materials: variation of structure and morphology and their use as metal-free catalysts, J. Mater. Chem. 18 (2008) 4893–4908.

[7] S. Kumar, V.R. Battula, K. Kailasam, Single molecular precursors for C_xN_y materials-Blending of carbon and nitrogen beyond g-C_3N_4, Carbon 183 (2021) 332–354.

[8] Q. Liang, B. Shao, S. Tong, Z. Liu, L. Tang, Y. Liu, M. Cheng, Q. He, T. Wu, Y. Pan, J. Huang, Z. Peng, Recent advances of melamine self-assembled graphitic carbon nitride-based materials: design, synthesis and application in energy and environment, Chem. Eng. J. 405 (2021) 126951.

[9] D. Mittal, D.P. Dutta, Synthesis, structure, and selected photocatalytic applications of graphitic carbon nitride: a review, J. Mater. Sci. Mater. Electron. 32 (2021) 18512–18543.

[10] A. Naseri, M. Samadi, A. Pourjavadi, A.Z. Moshfegh, S. Ramakrishna, Graphitic carbon nitride (g-C3N4)-based photocatalysts for solar hydrogen generation: recent advances and future development directions, J. Mater. Chem. 5 (2017) 23406–23433.

[11] T.R. Chetia, M.S. Ansari, M. Qureshi, Graphitic carbon nitride as a photovoltaic booster in quantum dot sensitized solar cells: a synergistic approach for enhanced charge separation and injection, J. Mater. Chem. 4 (2016) 5528–5541.

[12] R. Zhang, Y. Wang, Z. Zhang, J. Cao, Highly sensitive acetone gas sensor based on g-C3N4 decorated MgFe2O4 porous microspheres composites, Sensors 18 (2018).

[13] T. Lin, L. Zhong, J. Wang, L. Guo, H. Wu, Q. Guo, F. Fu, G. Chen, Graphite-like carbon nitrides as peroxidase mimetics and their applications to glucose detection, Biosens. Bioelectron. 59 (2014) 89–93.

[14] J. Liebig, Uber einige stickstoff - verbindungen, Ann. der. Pharm. 10 (1834) 1–47.

[15] L. Pauling, J.H. Sturdivant, The structure of cyameluric acid, hydromelonic acid and related substances, Proc. Natl. Acad. Sci. Unit. States Am. 23 (1937) 615–620.

[16] F. Dong, L.W. Wu, Y.J. Sun, M. Fu, Z.B. Wu, S.C. Lee, Efficient synthesis of polymeric g-C3N4 layered materials as novel efficient visible light driven photocatalysts, J. Mater. Chem. 21 (2011) 15171.

[17] G. Zhang, J. Zhang, M. Zhang, X. Wang, Polycondensation of thiourea into carbon nitride semiconductors as visible light photocatalysts, J. Mater. Chem 22 (2012) 8083.

[18] S.C. Yan, Z.S. Li, Z.G. Zou, Photodegradation performance of g-C3N4 fabricated by directly heating melamine, Langmuir 25 (2009) 10397.

[19] X. Wang, K. Maeda, A. Thomas, K. Takanabe, G. Xin, J.M. Carlsson, K. Domen, M. Antonietti, A metal-free polymeric photocatalyst for hydrogen production from water under visible light, Nat. Mater. 280 (2013) 967.

[20] C. Li, X. Yang, B. Yang, Y. Yan, Y. Qian, Synthesis and characterization of nitrogen-rich graphitic carbon nitride, Mater. Chem. Phys. 103 (2007) 427–432.

[21] R.C. Dante, P. Martín-Ramos, A. Correa-Guimaraes, J. Martín-Gil, Synthesis of graphitic carbón nitride by reaction of melamine and uric acid, Mater. Chem. Phys. 130 (2011) 1904, 1102.

[22] R.C. Dante, P. Martín-Ramos, F.M. Sánchez-Arévalo, L. Huerta, M. Bizarro, L.M. Navas-Gracia, J. Martín-Gil, Synthesis of crumpled nanosheets of polymeric carbon nitride from melamine cyanurate, J. Solid State Chem. 201 (2013) 153–163.

[23] X. Zhang, X. Xie, H. Wang, J. Zhang, B. Pan, Y. Xie, Enhanced photoresponsive ultrathin graphitic-phase C_3N_4 nanosheets for bioimaging, J. Am. Chem. Soc. 135 (2013) 18.

[24] H.B. Zheng, W. Chen, H. Gao, Y.Y. Wang, H.Y. Guo, S.Q. Guo, Z.L. Tang, J.Y. Zhang, Melem: an efficient metal-free luminescent material, J. Mater. Chem. C 5 (2017) 10746.

[25] H. Zheng, Z. Zhao, J.B. Phan, H. Ning, Q. Huang, R. Wang, J. Zhang, Wei Chen, Highly efficient metal-free two-dimensional luminescent melem nanosheets for bioimaging, ACS Appl. Mater. Interfaces 12 (2020) 2145–2151.

[26] R.C. Dante, P. Martín-Ramos, L.M. Navas-Gracia, F.M. Sánchez-Arévalo, J. Martín-Gil, Polymeric carbon nitride nanosheets, J. Macromol. Sci., Phys. 52 (2013) 623–631.

[27] P. Chamorro-Posada, A study of the therahertz spectra of crystalline materials (polyethylene, poly(vinylidene fluoride) form II, and a-D-Glucose) using NDDO semiempirical methods, J. Appl. Spectrosc. 85 (3) (2018). July.

[28] J.D.C. Maia, G.A. Urquiza Carvalho, C.P. Mangueira, S.R. Santana, L.A.F. Cabral, G.B. Rocha, J. Chem. Theor. Comput. 8 (2012) 3072–3081.

[29] P. Chamorro-Posada, J. Vázquez-Cabo, O. Rubiños-López, J. Martín-Gil, S. Hernández-Navarro, P. Martín-Ramos, F.M. Sánchez-Arévalo, A.V. Tamashausky, C. Merino-Sánchez, R.C. Dante, THz TDS study of several sp2 carbon materials: graphite, needle coke and graphene oxides, Carbon 98 (2016) 484–490.

[30] J. Ridley, M.C. Zerner, Theor. Chim. Acta 32 (1973) 111–134.

[31] A.D. Bacon, M.C. Zerner, Theor. Chim. Acta 53 (1979) 21–54.

[32] M.C. Zerner, G.H. Loew, R.F. Kirchner, U.T. Mueller-Westerhof, J. Am. Chem. Soc. 102 (1980) 589–599.

[33] J.J.P. Stewart, Optimization of parameters for semiempirical methods V: modification of NDDO approximations and application to 70 elements, J. Mol. Model. 173 (2007) 1173–1213.

[34] J. Ridley, M. Zerner, An intermediate neglect of differential overlap technique for spectroscopy: pyrrole and the azines, Theor. Chim. Acta 32 (1973) 111.

[35] M.C. Zerner, G.H. Loew, R.F. Kirchner, U.T. Mueller-Westerhoff, An intermediate neglect of differential overlap technique for spectroscopy of transition-metal complexes, Ferrocene, J. Am. Chem. Soc. 102 (1980) 589.

[36] F. Neese, The ORCA program system, Wiley Interdiscip. Rev. Comput. Mol. Sci. 2 (2012) 73.

[37] P.M. Lahti, J. Obrzut, F.E. Karasz, Use of the Pariser-Parr-Pople approximation to obtain practically useful predictions for electronic spectral properties of conducting polymers, Macromolecules 20 (1987) 2023–2026.

[38] J. Torras, J. Casanovas, C. Alemán, Reviewing extrapolation procedures of the electronic properties on the π-conjugated polymer limit, J. Phys. Chem. 116 (2012) 7571–7583.

[39] A. Zambon, J.-M. Mouesca, C. Gheorghiu, P.A. Bayle, J. Pécaut, M. Claeys-Bruno, S. Gambarelli, L. Dubois, s-Heptazine oligomers: promising structural models for graphitic carbon nitride, Chem. Sci. 7 (2016) 945–950.

[40] L. Duvillaret, F. Garet, J.L. Coutaz, A reliable method for extraction of material parameters in terahertz time-domain spectroscopy, IEEE J. Sel. Top. Quant. Electron. 2 (1996) 739–746.

[41] P.U. Jepsen, B.M. Fisher, Dynamic range in terahertz time-domain transmission and reflection spectroscopy, Opt. Lett. 30 (2005) 29–31.

[42] S.H. Baek, H.B. Lim, H.S. Chun, Detection of melamine in foods using terahertz time-domain spectroscopy," agric, Food Chem 62 (2014) 5403–5407.

[43] Y. Zheng, Z. Zhang, C. Lia, A comparison of graphitic carbon nitrides synthesized from different precursors through pyrolysis, J. Photochem. Photobiol. Chem. 332 (2017) 32–44.

[44] L.T.M. Oanha, L.T. Hang, N.D. Laid, N.T. Phuong, D.V. Thange, N.M. Hunge, D.D. Bich, N.V. Minh, Influence of annealing temperature on physical properties and photocatalytic ability of g-C3N4 nanosheets synthesized through urea polymerization in Ar atmosphere, Physica B 532 (2018) 48–53.

[45] T.-T. Pham, E.W. Shin, Influence of g-C3N4 Precursors in g-C3N4/NiTiO3 Composites on Photocatalytic Behavior and the Interconnection between g-C3N4 and NiTiO3e, Langmuir 34 (2018) 13144–13154.

[46] R.C. Dante, D.G. Dante, P. Martín-Ramos, P. Chamorro-Posada, M.C. Valsania, On an iridescent film of carbon nitride grown on an aluminum sheet and composed of overlapped oak-leaf shaped nanoparticles, Fullerenes, Nanotub. Carbon Nanostruct. (2021), https://doi.org/10.1080/1536383X.2021.2000401.

[47] V.W. Lau, B.V. Lotsch, A tour-guide through carbon nitride-land: structure- and dimensionality-dependent properties for photo(Electro)Chemical energy conversion and storage, Adv. Energy Mater. 12 (2022) 2101078.

[48] B.V. Lotsch, W. Schnick, From triazines to heptazines: novel nonmetal tricyanomelaminates as precursors for graphitic carbon nitride materials, Chem. Mater. 18 (2006) 1891–1900.

[49] B.V. Lotsch, W. Schnick, Thermal conversion of guanylurea dicyanamide into graphitic carbon nitride via prototype CNx precursors, Chem. Mater. 17 (2005) 3976–3982.

[50] B.V. Lotsch, W. Schnick, New light on an old story: formation of melam during thermal condensation of melamine, Chem. Eur J. 13 (2007) 4956–4968.

[51] P. Praus, A. Smýkalová, K. Foniok, V. Novák, J. Hrbac, Doping of graphitic carbon nitride with oxygen by means of cyanuric acid: properties and photocatalytic applications, J. Environ. Chem. Eng. 9 (2021), 105498.

[52] R.C. Dante, P. Martín-Ramos, A. Correa-Guimaraes, J. Martín-Gil, Synthesis of graphitic carbon nitride by reaction of melamine and uric acid, Mater. Chem. Phys. 130 (2011) 1094–1102.

[53] S. Liu, X.-Z. Song, G. Liu, Z. Dai, S. Zhang, C. Hao, Z. Tan, Synthesis of hollow donut-like carbon nitride for the visible light-driven highly efficient photocatalytic production of hydrogen and degradation of pollutants, New J. Chem. 44 (2020) 12247.